Wave-modulated orbits in rate-and-state friction

Thibaut Putelat[*,a,b], John R. Willis[b], Jonathan H.P. Dawes[c]

[a] *Laboratoire de Mécanique des Solides, UMR CNRS 7649, École Polytechnique, 91128 Palaiseau, France*
[b] *Institute of Theoretical Geophysics & Department of Applied Mathematics and Theoretical Physics University of Cambridge, Centre for Mathematical Sciences, Wilberforce Road, Cambridge CB3 0WA, U.K.*
[c] *Department of Mathematical Sciences, University of Bath, Claverton Down, Bath BA2 7AY, U.K.*

Abstract

A frictional spring–block system has been widely used historically as a model to display some of the features of two slabs in sliding frictional contact. Putelat, Dawes and Willis (2008) demonstrated that equations governing the sliding of two slabs could be approximated by spring–block equations, and studied relaxation oscillations for two slabs driven by uniform relative motion at their outer surfaces, employing this approximation. The present work revisits this problem. The equations of motion are first formulated exactly, with full allowance for wave reflections. Since the sliding is restricted to be independent of position on the interface, this leads to a set of differential-difference equations in the time domain. Formal but systematic asymptotic expansions reduce the equations to differential equations. Truncation of the differential system at the lowest non-trivial order reproduces a classical spring-block system, but with a slightly different "equivalent mass" than was obtained in the earlier work. Retention of the next term gives a new system, of higher order, that contains also some explicit effects of wave reflections. The smooth periodic orbits that result from the spring–block system in the regime of instability of steady sliding are "decorated" by an oscillation whose period is related to the travel time of the waves across the slabs. The approximating differential system reproduces this effect with reasonable accuracy when the mean sliding velocity is not too far from the critical velocity for the steady state. The differential system also displays a period-doubling bifurcation as the mean sliding velocity is increased, corresponding to similar behaviour of the exact differential-difference system.

Key words: rate-and-state friction, elastic wave, nonlinear dynamics, earthquake, slip stability, neutral delay differential equation
PACS:

[*] Corresponding author
Email addresses: putelat@lms.polytechnique.fr (Thibaut Putelat), J.R.Willis@damtp.cam.ac.uk (John R. Willis), J.H.P.Dawes@bath.ac.uk (Jonathan H.P. Dawes)

Contents

1. Introduction

Frictional spring–block systems have been studied for decades in search of a better understanding of friction. For practical and engineering interests, they also constitute good mechanical analogues of experimental apparatus, machines and tools. Moreover, they are useful "toy model" nonlinear systems for studying the dynamics of frictional stick-slip oscillations (Burridge and Knopoff, 1967, Rice and Tse, 1986) which represent a possible mechanism responsible for the recurrence of earthquakes (Brace and Byerlee, 1966). One could, however, argue legitimately that a spring–block system cannot "correspond closely to an actual fault" (Rice and Tse, 1986) whose behaviour depends on continuum mechanics fields.

In this paper, we present a method for reducing the dynamics of a frictional elastic continuum to the dynamics of a sliding block pulled with a generalized Kelvin–Voigt model (a spring and a dashpot in parallel) when elastic radiation and boundary reflection are accounted for. This particular aspect concerns only the modelling of the stress waves and is independent of the model of friction that is employed to complete the formulation. We thus propose a systematic method for deriving sliding–block mechanical analogues of frictional elastic continua that are useful for the investigation of the nonlinear dynamics of sliding friction and the states of erratic sliding of frictional systems and may provide new insight into the episodic recurrence of earthquakes and aftershocks.

Earthquakes are recurrent and aperiodic, while basic stick-slip oscillations are periodic. Experimentally, irregular slip patterns have been observed at very low driving velocities for which elastic radiation is commonly disregarded (Ruina, 1983, Gu et al., 1984, Gu and Wong, 1994). We will show that taking into account elastic radiation allows the appearance of complex slip dynamics even for low driving velocities.

Fully developed stick-slip oscillations are relaxation oscillations that comprise a long quasi-stationary phase[1] during which the stress builds up linearly in time followed by a sudden and short harmonic slip phase accompanied by a stress drop releasing the elastic energy stored during the first phase (Rice and Tse, 1986, Putelat et al., 2008). Although Coulomb's model of friction captures the essence of stick-slip oscillations from the difference in values between the static and dynamic coefficients of friction (Bowden and Tabor, 1954), it cannot account for the existence of a velocity-dependent critical value of the stiffness for the appearance of stick-slip and the increase of stick-slip amplitude for decreasing stiffness or velocity induced by slip memory effects (Rabinowicz, 1957). These experimental observations were reproduced theoretically, as we recall below, only from the concept of rate-and-state friction proposed by Ruina (1983) and Rice and Ruina (1983) following Dieterich (1979).

Rate-and-state friction is a general framework for the quantitative description of friction laws in which the frictional shear stress τ is determined by relations of the type

$$\tau = F(v, \phi; \sigma) \quad \text{and} \quad \dot{\phi} = -G(v, \phi; \sigma), \tag{1}$$

where v and σ denote the interfacial slip rate and normal stress while ϕ represents an internal variable characterising the state of resistance to sliding of the interface. The evolution law $(1)_2$ models the memory effects typical of the response of frictional interfaces to sudden velocity

[1] In this paper we define the "quasi-stationary phase" as the part of a periodic orbit on which the acceleration is negligible, reserving "quasi-static" for a part of an orbit, or a system, in which elastic wave propagation is disregarded.

changes. The instantaneous frictional response described by the law (1) implies the steady-state friction law

$$\tau = F_{ss}(V;\sigma), \tag{2}$$

obtained for slipping at constant rate $v = V$ and constant interfacial state $\phi = \phi_{ss}(V;\sigma)$ given implicitly by solving $G(V,\phi_{ss};\sigma) = 0$. Accounts of the phenomenological description and geophysical applications of such laws can be found in the review articles of Marone (1998) and Scholz (1998), while the present state of our physical understanding of such laws and their microphysical foundations are reviewed and discussed in Baumberger and Caroli (2006) and Putelat et al. (2011).

Phenomenologically, the concept of rate-and-state friction assumes that a reference value of the friction coefficient associated with a reference slip rate V_* is modified by correction terms that depend on the velocity and the interfacial state. It is supposed that the interfacial state relaxes to a steady state after sliding over a length characterised by a memory length L. A common realisation of such friction laws is the Dieterich ageing law defined by

$$\tau = [a_* + a\ln(v/V_*) + b\ln(\phi/\phi_*)]\,\sigma \quad \text{with} \quad \dot{\phi} = 1 - v\phi/L, \tag{3}$$

where $\phi_* = L/V_*$ is the steady-state reference value of the interfacial state. Typical values for the material parameters are given in Table 1. From a microphysical point of view the memory length is usually thought to correspond to the slip distance required for the rejuvenation of the population of interacting microasperities which constitute the interface topography (Dieterich, 1979, Dieterich and Kilgore, 1994, Baumberger and Caroli, 2006). Besides, in the thermodynamic theory for slip events based on the Eyring transition-state theory of rate processes (Heslot et al., 1994, Rice et al., 2001, Putelat et al., 2011), we note that the reference slip rate V_* can be identified as the product of a reference frequency of slip events and a characteristic length corresponding to the average separation between the energy barriers to overcome in relation to some thermal activation mechanism. We finally note that the analytical form of the state evolution law is empirical and is still open to discussion (see e.g. Putelat et al., 2011). We will use the law (3) to illustrate numerically the analyses reported in this paper.

Within this rate-and-state framework, consider a block of mass M pulled with a constant speed V by a spring of stiffness k. When friction is velocity-weakening, stick-slip motion arises from a Hopf bifurcation located at a critical value k_c of the stiffness given by

$$k_c = -G_\phi F'_{ss} + M\omega_c^2, \tag{4}$$

where

$$\omega_c^2 = -G_\phi^2 F'_{ss}/F_v, \tag{5}$$

denotes the critical frequency of oscillations (Rice and Ruina, 1983, Gu et al., 1984, Heslot et al., 1994, Putelat et al., 2010). The critical stiffness and frequency depend only on the velocity-dependent frictional properties of the interface, conveyed by the slope $F'_{ss}(V) < 0$ of the steady-state friction law and the partial derivatives $F_v \equiv \partial F/\partial v$ and $G_\phi \equiv \partial G/\partial\phi > 0$ evaluated at the steady state (V,ϕ_{ss}). We note that the inertia of the block promotes positive deviations from the quasi-static value $k_* = -G_\phi F'_{ss}$ of the critical stiffness at high frequency.

In Putelat et al. (2008), a first step towards connecting the dynamics of a slipping interface to the dynamics of a spring–block system was performed in the context of the problem illustrated in Fig. 1. Two horizontally infinite identical elastic slabs of thickness $h/2$ are driven in opposite directions with a uniform speed $V/2$ and slide against each other along a flat frictional interface

at $z = 0$ subjected to a normal stress σ. The density, the shear wave speed and the shear modulus of the slabs are denoted ρ, c_s and $\mathsf{G} = \rho c_s^2$ respectively. Assuming the interfacial slip to be uniform, the displacement in the two layers is horizontal and denoted $u(z,t)$, where z is the vertical coordinate. Assuming symmetry, it suffices to consider a velocity field in the upper layer of the form

$$\dot{u}(z,t) = V/2 + f\left(t - (z-h/2)/c_s\right) - f\left(t + (z-h/2)/c_s\right), \tag{6}$$

which accounts for shear waves radiating away from the interface and reflecting back from the top boundary. Equation (6) implies that the interfacial slip rate $v(t) = \dot{u}(0^+,t) - \dot{u}(0^-,t)$ and the rate of interfacial shear stress $\dot{\tau}(t)$ (from the time derivative of Hooke's law $\dot{\sigma}_{xz} = \mathsf{G}\dot{u}_z$) are given by

$$\left\{\begin{array}{rcl} v &=& V + 2[f(t+h/(2c_s)) - f(t-h/(2c_s))], \\ \dot{\tau} &=& -\rho c_s\,[f'(t+h/(2c_s)) + f'(t-h/(2c_s))]. \end{array}\right. \tag{7}$$

The complete system upon which the analysis of this paper is based comprises (7) together with the interfacial friction law (1), or equivalently after differentiating (1),

$$\dot{\tau} = F_v\dot{v} - GF_\phi, \quad \text{and} \quad \dot{\phi} = -G, \tag{8}$$

where the functions F_v, F_ϕ and G are evaluated at (v,ϕ,σ).

The analysis in this paper extends the analysis of Putelat et al. (2008) which proposed that (7) could be approximated by

$$\dot{\tau} = (\mathsf{G}/h)\,(V - v) - (\rho h/12)\,\ddot{v}, \tag{9}$$

by Taylor expanding the function f in the limit in which $t \gg h/c_s$. Equation (9) together with (1) describes the dynamics of a spring–block system of mass $M = \rho h/12$ and stiffness $k = \mathsf{G}/h$.

The contents of the paper are as follows. We revisit and improve on the analysis of Putelat et al. (2008) in section 2 where we describe a consistent procedure for reducing (7) to a system of ordinary differential equations (ODEs). The exact formulation (7) defines a differential-difference system of equations which is studied in section 3 within the framework of rate-and-state friction (1). In both cases, the linear stability of the steady-state sliding is presented together with leading order approximations of the quasi-stationary phase. Section 4 reports the results of some explicit computations using the Dieterich law (3). The stable periodic orbits that arise after a Hopf bifurcation from the steady-state solution for the exact system of differential-difference equations are reproduced with reasonable accuracy by the system of ODEs. Further results are then obtained for the ODE system, illustrating the complex dynamics facilitated by wave reverberations. Such results would be less easy to access for the exact system. Section 5 presents a few remarks in conclusion.

2. A spring–block mechanical analogue

2.1. Derivation

We assume that the interfacial slip rate varies very little during the time h/c_s with a view to Taylor expanding the functions $f(t \pm h/(2c_s))$ and $f'(t \pm h/(2c_s))$. Up to third order in h/c_s, this leads to the system

$$\left\{\begin{array}{rcl} 2(h/c_s)f'(t) + (h/c_s)^3 f'''(t)/12 &=& v - V, \\ 2f'(t) + (h/c_s)^2 f'''(t)/4 &=& -\dot{\tau}/(\rho c_s). \end{array}\right. \tag{10}$$

Further derivatives of f could be retained but keeping only those shown has the virtue that $f'(t)$ and $f'''(t)$ can be expressed solely in terms of $v(t)$ and $\tau(t)$.We remark that all such levels of approximation are singular perturbations in the sense that it is high-order derivatives that are lost. This in turn implies that we do not necessarily recover the dynamics of the delay-differential system from our asymptotic approximation in the limit $h/c_s \to 0$. Solving (10) and demanding for consistency that the double derivative of $f'(t)$ must equal $f'''(t)$ gives the "equation of motion" of the interface

$$\dot{\tau} = (\mathsf{G}/h)\,(V - v) - (\rho h/8)\,\ddot{v} - (h/c_s)^2\,\dddot{\tau}/24. \tag{11}$$

We recognize that (11) takes the form of the equation of motion for a block of mass $M = \rho h/8$ pulled at constant velocity V with a spring of stiffness $k = \mathsf{G}/h$ connected in parallel with a generalized 'dashpot' representing the radiative force

$$F_r = (h/c_s)^2\,\ddot{\tau}/24. \tag{12}$$

We use the analogy of a dashpot as we expect the friction force τ to depend on the slip velocity. We note that this radiative force generalises the radiative term $c_{\mathrm{rad}}\dddot{x}$ derived by Johansen and Sornette (1999).

We make contact with the work of Putelat et al. (2008) by noting that combining the double time derivatives of equations (10) in order to eliminate $f'''(t)$ provides us with the expression

$$\dddot{\tau} = -\rho c_s\,[(c_s/h)\ddot{v} + (h/c_s)^2\,f^{(5)}(t)/6],$$

which introduced into (11) gives

$$\dot{\tau} = (\mathsf{G}/h)\,(V - v) - (\rho h/12)\,\ddot{v} - \rho c_s\,(h/c_s)^4\,f^{(5)}(t)/144. \tag{13}$$

We thus see that the approximation $f'''(t) \approx (c_s/h)\ddot{v}/2$ proposed by Putelat et al. (2008), which neglects the term of order $(h/c_s)^3$ in the double time derivative of $(10)_1$, takes into account only the $\ddot{v}$ contribution of the radiative force. We will show later in the paper that the higher order term in $f^{(5)}$ in equation (13) is responsible in particular for fast oscillations during the slow quasi-stationary phase.

Choosing characteristic scales of length L, time L/V_* and stress σ, we write the interfacial stress in the form $\tau = \mu\sigma$, where μ is the coefficient of friction[2]. It is convenient, however, not to introduce further notation to replace V and v but to regard them instead to be measured in units of V_*. Equation (11) can then be expressed in the dimensionless form

$$r\,\dot{\mu} = \epsilon\,(V - v) - \epsilon r^2\,\ddot{v}/8 - r^3\,\dddot{\mu}/24, \tag{14}$$

where

$$\epsilon = \rho c_s V_*/\sigma \quad \text{and} \quad r = (h/c_s)/(L/V_*), \tag{15}$$

(recall $\mathsf{G} = \rho c_s^2$). This parametrisation reflects the fact that the normal stress σ and the system's thickness h are the two independent parameters that can be easily experimentally varied in addition to the driving velocity V, while the other quantities ρ, c_s and L, V_* represent respectively the material properties of the slabs and the interface and are supposed constant.

[2] As defined, μ depends in general on the normal stress σ.

We interpret ϵ as the ratio of the slab impedance ρc_s to the frictional impedance σ/V_* which measures the relative resistance of the wave propagation to the slip resistance of the interface. The second parameter corresponds to the ratio of the time h/c_s for the information carried by the elastic waves to be sent back to the interface after the boundary reflection to the characteristic time scale L/V_* of the interfacial state relaxation. It is necessary that $r \ll 1$ for the validity of the truncated Taylor expansions upon which the approximate equation (11) is based. We note that the dimensionless stiffness of the system

$$\kappa = kL/\sigma = \epsilon/r$$

is not independent of ϵ and r and would not be a suitable choice of parameter if we were to vary the system's thickness h.[3]

As an aside, we remark that the corresponding dimensionless form of the Dieterich ageing law (3) is

$$\left\{ \begin{array}{rcl} \mu & = & a_* + a\ln(v) + b\ln(\phi), \\ \dot{\phi} & = & 1 - v\phi. \end{array} \right. \tag{16}$$

Equation (14) with the friction law (8) constitute the system of differential equations which approximate the sliding dynamics of the interface when $r \ll 1$.

The system (14,8) can be expressed as a system of first-order differential equations. Writing $\dot{\mu} = \chi$ and $\delta = y - \mu$, where $\dot{y} = (\epsilon/r)(V - v)$, the system is of fourth order and can be written in the form

$$\left\{ \begin{array}{rcl} r\,\dot{\delta} & = & \epsilon\,(V - v) - r\,\chi, \\ \dot{\phi} & = & -G(v,\phi), \\ \dot{v} & = & [\chi + F_\phi(v,\phi)G(v,\phi)]/F_v(v,\phi), \\ r\,\dot{\chi} & = & 24\,\delta/r - 3\epsilon\,\dot{v}. \end{array} \right. \tag{17}$$

The new variable $\delta(t)$ denotes the difference between the spring force y and the friction force μ. We note that equation $(17)_4$ corresponds to a time integration of (14) with initial condition $\delta(0) = y(0) - \mu(0) = \epsilon\, r\,\dot{v}(0)/8 + r^2\,\ddot{\mu}(0)/24$, in order to ensure that, in steady state, friction balances the elastic spring force so that $\mu_{ss}(V) = y$.

We observe that the usual quasi-static limit in which wave propagation is disregarded corresponds to the limit $r \to 0$ which implies that $y = \mu$ from $(17)_4$, and hence $\dot{\mu} = \dot{y}$, reducing (17) to

$$\left\{ \begin{array}{rcl} \dot{\mu} & = & (\epsilon/r)\,(V - v), \\ \dot{\phi} & = & -G(v,\phi), \end{array} \right.$$

where the interfacial slip rate $v(\mu,\phi)$ is obtained directly by solving $(1)_1$ for v.

2.2. Linear stability of steady-state sliding

The possible growth rates s of infinitesimal perturbations of the steady-state solution of (17),

$$(\delta,\phi,v,\chi) = (0,\phi_{ss},V,0),$$

are given by the eigenvalues s of the 4×4 Jacobian matrix of (17) which are the roots of the quartic

$$rs[1 + (rs)^2/24](F_v s + G_\phi F'_{ss}) + \epsilon\,[1 + (rs)^2/8](s + G_\phi) = 0, \tag{18}$$

[3] Using dimensionless ratios κ and r, equation (14) would read $\dot{\mu} = \kappa\,(V - v) - (\kappa\, r^2/8)\,\ddot{v} - (r^2/24)\,\dddot{\mu}$.

where the derivatives F'_{ss}, F_v, G_ϕ are evaluated at $(\phi, v) = (\phi_{ss}, V)$.

Steady-state motion becomes unstable as r increases, when a root of (18) first acquires a positive real part; the corresponding critical value $\tilde{r}_c$ of r is that for which a root has zero real part. The simplest possibility, that $s = 0$, can never happen since $\epsilon G_\phi > 0$. It is appropriate, therefore, to investigate the possibility of a Hopf bifurcation, for which a pair of complex conjugate roots become pure imaginary, say $s = \pm i\omega_c$. Substituting these values into the quartic equation (18) and taking real and imaginary parts gives

$$\begin{cases} -rF_v[1-(r\omega_c)^2/24]\omega_c^2 + \epsilon G_\phi[1-(r\omega_c)^2/8] &= 0 \\ rG_\phi F'_{ss}[1-(r\omega_c)^2/24] + \epsilon[1-(r\omega_c)^2/8] &= 0 \end{cases} \tag{19}$$

when the parameter is critical $r = \tilde{r}_c$. Their combination gives the frequency at criticality

$$\omega_c^2 = -G_\phi^2 F'_{ss}/F_v, \tag{20}$$

which, when inserted in $(19)_2$, yields the polynomial

$$\tilde{r}_c^3 - 3r_*\,\tilde{r}_c^2 - (24/\omega_c^2)\,\tilde{r}_c + (24/\omega_c^2)\,r_* = 0, \tag{21}$$

determining the critical value of the parameter r, where we have defined

$$r_* = -\epsilon/(G_\phi F'_{ss}), \tag{22}$$

the quasi-static value of the critical r. The cubic equation (21) can be solved explicitly; there are several equivalent forms available in which to present the roots. Employing the notation

$$p = r_*^3, \quad q = r_*^2 + 8/\omega_c^2, \tag{23}$$

the roots are

$$r_* + i\sqrt{3}(r_1 - r_2)/2 - (r_1 + r_2)/2, \quad r_* - i\sqrt{3}(r_1 - r_2)/2 - (r_1 + r_2)/2, \quad r_* + r_1 + r_2, \tag{24}$$

where

$$r_1 = [p + i(q^3 - p)^{1/2}]^{1/3}, \quad r_2 = [p - i(q^3 - p)^{1/2}]^{1/3}. \tag{25}$$

Thus, the roots are real, and are written in ascending order in (24). The smallest root has to be negative while the other two are positive. The relevant root is therefore the intermediate one,

$$\tilde{r}_c = r_* - i\sqrt{3}(r_1 - r_2)/2 - (r_1 + r_2)/2, \tag{26}$$

since this is encountered first as r increases from zero. It is interesting to rewrite $\tilde{r}_c$ as

$$\tilde{r}_c = r_* + 2r_*\,\sin(\theta/3 - \pi/6)/\cos^{1/3}(\theta) \tag{27}$$

with $\theta = \tan^{-1}(\sqrt{\alpha})$ where we define $\alpha = (1 + 8/(r_*\omega_c)^2)^3 - 1 > 0$. We note that the quasi-static limit is then obtained for $\theta \to \pi/2$ which corresponds to the condition $r_*\omega_c \to 0$.

Finally we can conclude that the steady-state sliding is stable when $r < \tilde{r}_c$, the four roots of the quartic equation having negative real parts. At $r = \tilde{r}_c$ the two least stable complex conjugate roots cross the imaginary axis. The dash-dotted line in Figure 2 represents $\tilde{r}_c$ as defined by (27) for the Dieterich law, and using the parameter values for paper given in Table 1.

A complementary way of looking for the critical r is to find the stability boundary in the parameter plane (r, ϵ) defined by (21) and (22), i.e.

$$\tilde{\epsilon}_c = -G_\phi F'_{ss}\, r\, \frac{r^2 - 24/\omega_c^2}{3(r^2 - 8/\omega_c^2)}. \tag{28}$$

The term $-G_\phi F'_{ss}\, r$ would be the value ϵ to reach criticality under the quasi-static limit. It corresponds to the asymptote of $\tilde{\epsilon}_c$ as $r \to 0$. $\tilde{\epsilon}_c$ is not defined for $\sqrt{8}/\omega_c < r < \sqrt{24}/\omega_c$. The boundary $\tilde{\epsilon}_c$ for $r > \sqrt{24}/\omega_c$ corresponds to a second pair of complex conjugate roots crossing the imaginary axis. The stability boundary (28) for the Dieterich law is shown by the dash-dotted line in Figure 3.

3. Differential-difference formulation

3.1. Formulation

The exact differential-difference formulation of the single interface problem is given by the combination of the wave and interface dynamics (7) and rate-and-state friction (1). We begin by time-shifting the undetermined function f by defining $g(t) = f(t + h/(2c_s))$ so that system (7) reads

$$\left\{ \begin{array}{rcl} v(t) & = & V + 2[g(t) - g(t - h/c_s)], \\ \dot{\tau} & = & -\rho c_s[g'(t) + g'(t - h/c_s)]. \end{array} \right. \tag{29}$$

We also suppose that a curve of initial data $\gamma(t)$ is specified:

$$g(t) = \gamma(t) \quad \text{for} \quad -h/c_s \leqslant t \leqslant 0. \tag{30}$$

We will denote $g(0)$ and $\gamma(0)$ the limits from the right and from the left of the functions g and γ respectively. In the general theory of differential-difference equations (Bellman and Cook, 1953) it is possible to introduce initial jumps $g(0) \neq \gamma(0)$.

Then the time integration of $(29)_2$ combined with the rate-and-state equation (1) gives the algebraic-differential-difference system

$$\left\{ \begin{array}{rcl} \tau_{ss}(V) - \rho c_s[g(t) + g(t - h/c_s)] & = & F[V + 2[g(t) - g(t - h/c_s)], \phi], \\ \dot{\phi} & = & -G[V + 2[g(t) - g(t - h/c_s)], \phi], \end{array} \right. \tag{31}$$

which determines the dynamics of the interface. Importantly, we have assumed that the initial conditions involved in the time integration of $(29)_2$ satisfy

$$\tau(0) + \rho c_s[g(0) + \gamma(-h/c_s)] + \rho c_s\,[g(0) - \gamma(0)] = \tau_{ss}(V), \tag{32}$$

in order to allow the possibility of a steady-state solution for (31) associated with no elastic radiation, i.e. $g(t) \equiv 0$.

As a result, formulation (31) suggests that the unknown wave function $g(t)$ combines with its retarded value $g(t - h/c_s)$ to define the perturbations of stress and velocity

$$\delta\tau(t) := -\rho c_s[g(t) + g(t - h/c_s)] \quad \text{and} \quad \delta v(t) := 2[g(t) - g(t - h/c_s)]$$

of the steady sliding state of the interface. Given the initial perturbations $\delta\tau_0 \equiv \delta\tau(0) = -\rho c_s[g(0) + \gamma(-h/c_s)]$ and $\delta v_0 \equiv \delta v(t) = 2[g(0) - \gamma(-h/c_s)]$, we can write the initial conditions required for the forward time integration of (31) as

$$g(0) = -\delta\tau_0/(2\rho c_s) + \delta v_0/4, \tag{33}$$

with the initial value of the interfacial state $\phi(0)$ obtained from the inversion of the friction law

$$F[V + \delta v_0, \phi(0)] = \tau_{ss}(V) + \delta\tau_0. \tag{34}$$

Finally, we nondimensionalise using the same characteristic scales as in section 2: length L, time L/V_* and stress σ. The dimensionless form of (31) is

$$\begin{cases} \tau_{ss}(V) - \epsilon\,[g(t) + g(t-r)] &= F[V + 2[g(t) - g(t-r)], \phi], \\ \dot{\phi} &= -G[V + 2[g(t) - g(t-r)], \phi], \end{cases} \tag{35}$$

where $\epsilon = \rho c_s V_*/\sigma$ and $r = (h/c_s)/(L/V_*)$ are defined exactly as in (15). The natural interpretation is that ϵ measures the magnitude of the stress perturbation while r is the single (and constant) dimensionless delay time for this differential-difference system.

3.2. Linear stability of steady-state sliding

We consider a small perturbation of the steady-state solution $(g, \phi) = (0, \phi_{ss}(V))$ of (35) such that $g = \hat{g}$ and $\phi = \phi_{ss} + \hat{\phi}$. The stability of the steady-state sliding of the interface is governed by the equations (linearised in $\hat{g}$ and $\hat{\phi}$):

$$\begin{cases} -\epsilon\,[\hat{g}(t) + \hat{g}(t-r)] &= 2F_v\,[\hat{g}(t) - \hat{g}(t-r)] + F_\phi\,\hat{\phi}, \\ \dot{\hat{\phi}} &= -2G_v\,[\hat{g}(t) - \hat{g}(t-r)] - G_\phi\,\hat{\phi}, \end{cases} \tag{36}$$

where the partial derivatives of F and G with respect to v and ϕ, denoted F_v, F_ϕ, G_v and G_ϕ, are evaluated at $(v, \phi) = (V, \phi_{ss})$.

A non-trivial solution of (36) with time-dependence e^{st} is possible if the growth rate s satisfies the transcendental characteristic equation

$$Q(s, r) = A(s) + C(s)\,\mathrm{e}^{-sr} = 0 \tag{37}$$

where $A(s) = (F_v + \epsilon/2)s + G_\phi(F'_{ss} + \epsilon/2)$ and $C(s) = -(F_v - \epsilon/2)s - G_\phi(F'_{ss} - \epsilon/2)$. Since the polynomials $A(s)$ and $C(s)$ are of the same degree, the differential-difference system is termed 'neutral' (Bellman and Cook, 1953). This means that the current rate of change of the function g, which in turn determines the rate of change of the interfacial stress, depends on the past rate of change of g in addition to the past and current values of g (see equation (29)). We note that the quartic equation (18) cannot be recovered from the series expansion of (37) for $r \to 0$ since this is a singular limit as far as the asymptotic expansion in section 2 is concerned.

Study of solutions to (37) shows that in the quasi-static limit $r \to 0$ steady-state sliding is stable. As the delay r increases, a pair of complex conjugate roots $s = s_r \pm i\omega$ crosses the imaginary axis from the left half plane to the right half plane with the frequency

$$\omega_c^2 = -G_\phi^2 F'_{ss}/F_v, \tag{38}$$

when the delay r reaches the critical value

$$r_c = \frac{\tan^{-1}(r_*\omega_c/2)}{\omega_c/2}, \tag{39}$$

where we recall that $r_* = -\epsilon/(G_\phi F'_{ss})$. The critical frequency ω_c depends only on the friction law; given this fact it is not surprising that the same value was obtained from the approximate

ODE formulation. However, the critical value of r is different. The solid line in Figure 2 shows r_c given by (39), together with its approximation $\tilde{r}_c$ given by (27), shown dash-dotted, for the Dieterich law. As mentioned previously, in this and all succeeding figures, the parameter values were chosen as those shown for paper in Table 1. The approximation $\tilde{r}_c$ follows the exact stability boundary very closely. The right-hand plot in Figure 2 shows that the relative error is very small for $V < 10^3 V_*$ but grows to the order of 10% as V approaches $10^6 V_*$.

The quasi-static approximation $r_c = r_* \equiv -\epsilon/(G_\phi F'_{ss})$ is recovered in the limit $r_* \omega_c \to 0$. As for the spring–block analogue and the boundary (28), expression (39) gives the stability boundary in the parameter plane (ϵ, r)

$$\epsilon_c = -G_\phi F'_{ss} \frac{\tan(r\,\omega_c/2)}{\omega_c/2}. \tag{40}$$

As a result, steady-state slidings are unstable when the delay $r > r_c$ or alternatively if $\epsilon < \epsilon_c$. Figure 3 compares the approximate and exact stability boundaries in the (r, ϵ) plane for the Dieterich law.

Interestingly, in the quasi-static limit $r_* \omega_c \to 0$, the series expansion of (39) leads to

$$\kappa_c = \epsilon/r_c = \kappa_* + \epsilon r_*\, \omega_c^2/12 + \cdots$$

where $\kappa_* \equiv \epsilon/r_* = -G_\phi F'_{ss}$ is the quasi-static dimensionless stiffness. We recognize the classical critical stiffness of a spring–block system (4) whose dimensionless mass $m = \epsilon r_*/12$ corresponds to the approximation studied in Putelat et al. (2008) based on equation (9).

4. An illustrative example

In this section we present numerical results using the Dieterich ageing law (3). For the ODE system, the results are obtained with the continuation package AUTO (Doedel et al., 1991); for the time integration of differential-difference equations they are obtained using the package RADAR5 V2.1 (Guglielmi and Hairer, 2001, 2005). Adopting the Dieterich ageing law, the ODE system comprises (14) together with (16). It was found convenient for the computations to express the first-order system (17,16) in the form

$$\left\{ \begin{array}{lcl} \mu' &=& r\chi, \\ y' &=& \epsilon\,(V - v), \\ w' &=& r(10^{-w} - v)/\ln(10), \\ \chi' &=& [24(y - \mu) - 3\epsilon v']/r, \end{array} \right. \tag{41}$$

where time has been rescaled so that $\hat{t} = t/r$ and $(\cdot)' = d(\cdot)/d\hat{t}$, $w = \log_{10}(\phi)$ and

$$v = \exp[(\mu - a_* - b\ln(10)w)/a] \quad \text{so that} \quad v' = (v/a)(\mu' - b\ln(10)w'), \tag{42}$$

from $(16)_1$.

Computations were performed for $V = 100 V_*$ and $\epsilon = 2.8 \times 10^{-5}$. For these values, the critical value $\tilde{r}_c$ for the ODE system is very close to the critical value $r_c \approx 10^{-2.699}$ for the differential-difference system (see Figure 2).

Figure 4 shows plots relating to the stable periodic orbit that results when $r = 10^{-2.68}$, slightly greater than r_c. In the units (h/c_s) employed for t, the period for this value of r is $T_{\text{ode}} \approx 70.73$. The new feature introduced by the ODE formulation (14) compared to the spring–block formulation (9) of Putelat et al. (2008) is the occurrence of fast oscillations superimposed on

the slow increase of the interfacial stress $\tau = \mu\sigma$ during the quasi-stationary phase. The fast oscillations can be understood from equation (14) which behaves at leading order like

$$r^2\,\dddot{\mu}/24 + \dot{\mu} \approx (\epsilon/r)\,V,$$

since the inertial term $\epsilon r\,\ddot{v}/8$ and the interfacial slip rate $v \ll V$ are negligible over the quasi-stationary phase. We see that the slow linear ramp results from the quasi-static elastic contribution $(\epsilon/r)\,V$ (see Putelat et al. (2008) for more details) while the fast oscillations originate from wave reverberations. This leading order approximation yields an estimate for the frequency of $\omega_v = 2\sqrt{6}/r$ and hence an oscillation period of

$$T_v = \pi\, r/\sqrt{6} \approx 1.28\, r, \tag{43}$$

which is clearly set by the delay induced by the reflection of the waves radiated from the frictional interface. We note that these oscillations are intrinsic to the formulation (14). They correspond to natural oscillations of the system determined by its thickness and do not depend on the details of the friction force. The frictional properties of the interface will determine, in response to this forcing, the very low speed sliding.

No corresponding figure is shown but the same conclusion is reached from the delay formulation (29) although in the delay case the vibration period is exactly the delay r. In the quasi-stationary phase where $v \ll V$, at leading order, the unknown function g solves the first order linear difference equation $g(t) \approx g(t-r) - V/2$ obtained from $(29)_1$. Its solution is

$$g(t) = -Vt/(2r) + \gamma(t),$$

where $\gamma(t)$ is any r-periodic function that satisfies $g(0) = \gamma(0)$. The interfacial stress follows from inserting this leading-order approximation for $g(t)$ into $(35)_1$ to obtain

$$\tau(t) = \epsilon Vt/r - 2\epsilon\,\gamma(t) + \tau_{ss}(V) - \epsilon V/2.$$

Solutions for the ODE formulation and the exact DDE formulation are compared in Figure 5. The figure includes corresponding plots for the spring–block approximations with $M = \rho h/8$ (obtained from (14)) and with $M = \rho h/12$ as developed by Putelat et al. (2008). These cannot, of course, exhibit the rapid oscillations but follow the exact orbit "on average", with $M = \rho h/8$ being perhaps the closer of the two. The full ODE approximation has all the correct qualitative features. Quantitatively, however, the period of the exact orbit for the parameters used in Figure 5 is $T_{dde} \approx 73.5$ and, as observed above, the frequency of the fast oscillations for the ODE system is about 28% too high.

The periodic orbit itself undergoes a bifurcation and becomes unstable as r increases. Numerical bifurcation theory for DDEs is less developed than that for ODEs, and the continuation code RADAR5 for the DDE formulation provides less information than AUTO does for the ODE approximation. We therefore present detailed results for the ODE formulation and anticipate that the DDE formulation will display similar features. A detailed study of the DDE formulation will be the subject of future work.

Figure 6 shows bifurcation diagrams for the ODE system, with $V = 100V_*$ and $\epsilon = 2.8 \times 10^{-5}$. The first feature to notice is the initial Hopf bifurcation from the steady-state solution, at $r \approx 10^{-2.699}$. The bifurcation is very mildly subcritical and gives birth to an unstable primary periodic orbit which then restabilizes at a saddle-node bifurcation (not distinguishable in Fig. 6).

The subcritical or supercritical nature of the Hopf bifurcation appears broadly to be preserved between the spring–block approximation and the ODE formulation (see Putelat et al. (2010) for a detailed weakly nonlinear analysis of the Hopf bifurcation of a spring–block system).

Figure 6(a) shows two sets of curves. The upper set gives the bifurcation diagram for the interfacial stress drop $\Delta\mu = \mu_{\max} - \mu_{\min}$, together with those for the two spring–block approximations, while the lower set gives the diagram for the elastic stress drop $\Delta y = y_{\max} - y_{\min}$. The noticeable difference between the amplitudes of $\Delta\mu$ and of Δy is caused by the fast oscillations of the instantaneous interfacial stress around its average value y during the quasi-stationary phase. Even when inertia is negligible, the equation of motion (14), written with respect to the short time scale $\hat{t} = t/r$,

$$3\epsilon v' = 24(y - u) - \mu''$$

reveals that $\mu \neq y$ along a cycle because of the radiative term, conversely to the spring–block approximations. The "smooth" cycles produced by these latter provide an envelope for the stick-slip cycle of the Kelvin–Voigt approximation. Figure 6(a) also presents estimations of $\Delta\mu$ and Δy for the exact DDE system.[4] In both cases the exact stress drops are larger than those given by the ODE approximations, with a relative error which increases with r.

Along the primary branch of periodic solutions (cf. Fig. 6(b)), several connected period-doubling bifurcations separated by saddle-node bifurcations are found until a torus bifurcation is encountered (at $r_{TR} = 10^{-2.468}$ for $V = 100\,V_*$ and $\epsilon = 2.8 \times 10^{-5}$) from which the periodic orbits never become stable again for larger value of the delay. Figure 6(b) gives a blow-up of the bifurcation diagram for Δy, that shows more clearly the development of complex dynamics through successive period-doubling bifurcations. Figure 7 illustrates both the unstable periodic orbit and the stable period-doubled orbit after the first period-doubling bifurcation, at the parameter value $r = 10^{-2.59}$. The period of the unstable orbit is $T_{\text{ode}} \approx 79.09$. The upper graph shows slip velocity v against time, normalized to the relevant period ($T = T_{\text{ode}}$ for the unstable orbit and $T = 2T_{\text{ode}}$ for the period-doubled orbit). In real time, the peak velocity for the unstable orbit would appear twice, superimposed on the two slightly different peaks realized by the period-doubled orbit. The lower figure plots the projections of the orbits on the (μ, v) plane and demonstrates how the period-doubled orbit is close but not identical to two successive traces of the unstable periodic orbit.

Figure 8 presents the delay dependence of the stick-slip period of the primary periodic orbit. Compared with the period of the spring–block approximations, we emphasize that the wave reverberation induces lower period values in relation to the loss of energy used for the fast oscillations during the quasi-stationary phase. Because the period of the stick-slip oscillation is proportional to the elastic stress drop Δy (Putelat et al., 2008)

$$T_{\text{stick-slip}} \sim \frac{\Delta y}{(\epsilon/r)V},$$

the amplitude reduction of Δy shortens the recurrence time of slip events of the elastic layers. Its estimation for the DDE formulation was further obtained from the direct numerical integration of system (41) with RADAR5 for different values of the delay. It is found that the stick-slip period of the DDE formulation is intermediate to the ODE and spring-block approximations

$$T_{\text{ode}} < T_{\text{dde}} < T_{\text{spring-block}}.$$

[4] The elastic stress drop is calculated from the numerical quadrature in time of $y' = \epsilon(V - v)$ for which the slip rate v is provided by $(29)_1$, the function g being computed with RADAR5.

Finally, when r is chosen further inside the stick-slip domain, i.e. for values of the delay larger than the value at which a torus bifurcation occurs on the primary periodic orbit, some features of complex stick-slip patterns can be found as displayed in Figure 9. Using direct numerical time integration for both the ODE and DDE systems with $r = 10^{-2.3}$, $V = 100\,V_*$ and $\epsilon = 2.8 \times 10^{-5}$, Figure 9 also exposes the limitations of the ODE approximation. The temporal patterns are different for the two systems. With variable interfacial stress drops associated with variable velocity slip events, the ODE approximation looks more irregular (cf. Fig. 9(a)) than the exact DDE system whose cycles share some similarities, disregarding the quasi-stationary fast oscillations, with the spring–block relaxation oscillations described in Putelat et al. (2008) at a first glance (cf. Fig. 9(b)). For this value of the delay, the DDE cycles are characterised by rather constant interfacial stress drop amplitudes combined with small amplitude slip rate oscillations around the steady-state line during the inertial phase. The fast oscillations decorating the quasi-stationary phase show new structures, whose shapes moreover vary from one quasi-stationary phase to another. On the contrary, the ODE cycles exhibit inertial phases marked by stick-slip like high amplitude oscillations while the quasi-stationary fast oscillations remain sinusoidal, although of different amplitude between subsequent quasi-stationary phases.

5. Conclusion

The main thrust of this paper is to develop a systematic extension of the dynamics of a frictional interface that includes the effects of elastic waves propagating through the (thin) slabs either side of the interface and reflecting from the outer boundaries of the slabs. This results in a system of nonlinear differential-difference equations that are difficult to treat mathematically.

We then derive, more systematically than in Putelat et al. (2008), ordinary differential equation approximations to the exact differential-difference equations. The lowest non-trivial order approximation provides a slight correction for the mass term in the approximating mass–spring system developed in Putelat et al. (2008); it also produces the leading-order term that is required to account for wave reflections. Approximations of higher order could be developed quite easily but these would contain derivatives of the wave function f as internal variables, in addition to the "physical" interface variables τ, v and ϕ. Approximations of this type could also be developed for other problems involving one or more thin layers. The potential advantage of such approximations is that the theory of nonlinear ODEs is very well advanced, and detailed numerical results relating to the development of complex dynamics can be obtained using existing code such as AUTO.

We find that the nonlinear frictional dynamics of two identical elastic slabs is governed, in addition to the slab driving velocity, by the relative impedance $\epsilon = \rho c_s V_*/\sigma$ and the relative reverberation time $r = (h/c_s)/(L/V_*)$. These two dimensionless parameters highlight the role of the interfacial state relaxation time-scale L/V_* and the frictional impedance σ/V_* in the occurrence of stick-slip oscillations and their control by the interfacial microstructure evolution processes. We show that the steady slipping mode of the frictional interface is destabilized when the system's reverberation time is large compared to the critical delay (39), or equivalently, when the system's relative impedance is smaller than the critical impedance (40); critical values which define a surface in the three-dimensional parameter space (V, r, ϵ). Regarding the stick-slip oscillations, we find that the slabs' inertia involved in the wave reverberation drives fast oscillations during the quasi-stationary phase of the stick-slip cycle. Their amplitude is significant compared to the stress drops which accompany the slip events of the inertial phase. In the present formulation, these fast oscillations do not fade away over the stick-slip cycle because of the absence

of further energy loss. Interesting extensions of this work would then include the addition of a visco-elastic component for the behaviour of the slabs, and the inclusion of only partial reflection of the elastic waves at the system boundaries. Overall we conclude that wave propagation cannot be neglected for the stick-slip dynamics of such a continuum.

In detail, the ODE approximation that we develop here is shown to reflect accurately properties of the exact system such as the critical delay (r_c) for the onset of the Hopf bifurcation from the steady-state solution, and its frequency. It also provides a good picture of the oscillations produced by wave reverberations, although these do not have quite the correct frequency. Period-doubling bifurcations arise and are easily detected (numerically) in the ODE system (they are less easily accessible in the exact DDE system). Such a collection of period-doubling bifurcations does not occur for the spring–block approximation. Wave reflections thus provide one credible mechanism for the development of complex dynamics of interfacial slip. We remark finally that our work retained an assumption of symmetric wave propagation above and below the interface. It appears that relaxation of this restriction could be made, but at the expense of producing a system with additional variables that cannot be expressed solely in terms of the "physical" variables that are defined on the interface.

Acknowledgements

JHPD gratefully acknowledges financial support from the Royal Society through a University Research Fellowship.

References

Baumberger, T. and Caroli, C. (2006). Solid friction from stick-slip down to pinning and aging. *Adv. in Phys.*, 55:279–348.

Bellman, R. and Cook, K. L. (1953). *Differential-Difference Equations*, volume 6 of *Mathematics in Engineering*. Academic Press.

Bowden, F. P. and Tabor, D. (1954). *The Friction and Lubrication of Solids*. Oxford - Clarendon Press.

Brace, W. F. and Byerlee, J. D. (1966). Stick slip as a mechanism for earthquakes. *Science*, 153:990–992.

Burridge, R. and Knopoff, L. (1967). Model and theoretical seismicity. *Bull. Seismol. Soc. Am.*, 57:341–371.

Dieterich, J. H. (1979). Modeling rock friction: 1. experimental results and constitutive equations. *J. Geophys. Res.*, 84:2161–2168.

Dieterich, J. H. and Kilgore, B. D. (1994). Direct observation of frictional contacts: new insights for state-dependent properties. *Pageoph.*, 143:283–302.

Doedel, E. J., Keller, H. B., and Kernevez, J. P. (1991). Numerical analysis and control of bifurcation problems. *Int. J. Bifurcation and Chaos*, 1(3):493–520. AUTO 2000 available via Internet from http://indy.cs.concordia.ca/auto/.

Gu, J. C., Rice, J. R., Ruina, A. L., and Tse, S. T. (1984). Slip motion and stability of a single degree of freedom elastic system with rate and state dependent friction. *J. Mech. Phys. Solids*, 32:167–196.

Gu, Y. and Wong, T.-F. (1994). Nonlinear dynamics of the transition from stable sliding to cyclic stick-slip in rock. In Newman, W., Gabrielov, A., and Turcotte, D., editors, *Nonlinear Dynamics and Predictabilitiy of Geophysical Phenomena*, number 83 in IUGG Geophysical Monograph, pages 15–35. American Geophysical Union.

Guglielmi, N. and Hairer, E. (2001). Implementing Radau IIA methods for stiff delay differential equations. *Computing*, 67:1–12.

Guglielmi, N. and Hairer, E. (2005). Users guide for the code RADAR5 — Version 2.1. Technical report, University of Geneva. http://www.unige.ch/~hairer/software.html.

Heslot, F., Baumberger, T., Perrin, B., Caroli, B., and Caroli, C. (1994). Creep, stick-slip, and dry-friction dynamics: Experiments and a heuristic model. *Phys. Rev. E*, 49:4973–4988.

Johansen, A. and Sornette, D. (1999). Acoustic radiation controls dynamic friction: evidence from a spring–block experiment. *Phys. Rev. Lett.*, 82:5152–5155.

Marone, C. (1998). Laboratory-derived friction laws and their application to seismic faulting. *Annu. Rev. Earth Sci.*, 26:643–696.

Putelat, T., Dawes, J. H. P., and Willis, J. R. (2010). Regimes of frictional sliding of a spring-block system. *J. Mech. Phys. Solids*, 58:27–53.

Putelat, T., Dawes, J. H. P., and Willis, J. R. (2011). On the microphysical foundations of rate-and-state friction. *J. Mech. Phys. Solids*, 59:1062–1075.

Putelat, T., Willis, J. R., and Dawes, J. H. P. (2008). On the seismic cycle seen as a relaxation oscillation. *Phil. Mag.*, 88:3219–3243.

Rabinowicz, E. (1957). The intrinsic variables affecting the stick-slip process. *Proc. Phys. Soc. (London)*, 71:668–675.

Rice, J. R., Lapusta, N., and Ranjith, K. (2001). Rate and state dependent friction and the stability of sliding between elastically deformable solids. *J. Mech. Phys. Solids*, 49:1865–198.

Rice, J. R. and Ruina, A. L. (1983). Stability of steady frictional slipping. *J. Appl. Mech.*, 50:343–349.

Rice, J. R. and Tse, S. T. (1986). Dynamic motion of a single degree of freedom system following a rate and state dependent friction law. *J. Geophys. Res.*, 91(B1):521–530.

Ruina, A. (1983). Slip instability and state variable friction laws. *J. Geophys. Res.*, 88:10,359–10,370.

Scholz, C. H. (1998). Earthquakes and friction laws. *Nature*, 391:37–41.

List of Figures

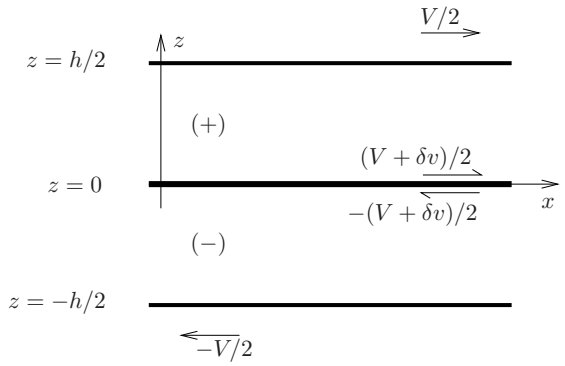

Figure 1: A single interface system: two identical elastic slabs slide in opposite directions at constant speed $\pm V/2$; elastic shear waves radiate from the frictional interface and reflect at the boundaries $z = \pm h/2$.

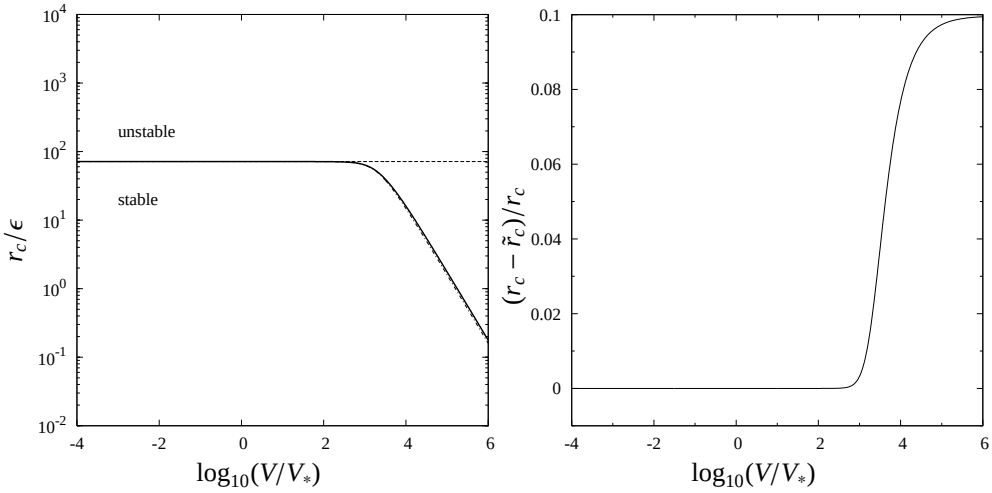

Figure 2: The left-hand side graphic corresponds to the regime diagram of the sliding stability of the single interface under the Dieterich law: the solid line represents the critical delay r_c (39) of the differential-difference system; the dash-dotted line represents its approximation $\tilde{r}_c$ (27) from the spring–block equation; the dashed line corresponds to the quasi-static value (22). The right-hand side graphic shows the relative error between the critical delay (27) and (39). Parameters: $\epsilon = \rho c_s V_*/\sigma = 2.8 \times 10^{-5}$ ($\sigma = 10^3$ Pa).

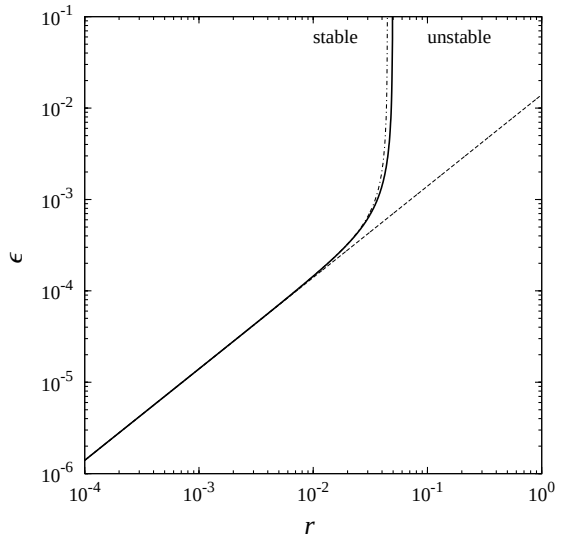

Figure 3: Stability boundaries (28) (dash-dotted line) and (40) (solid line) for the Dieterich law at $V/V_* = 100$. Dashed line: quasi-static stability boundary (22). When V/V_* increases, the vertical asymptote $r = \sqrt{8}/\omega_c$ moves to the left, reducing the stability domain.

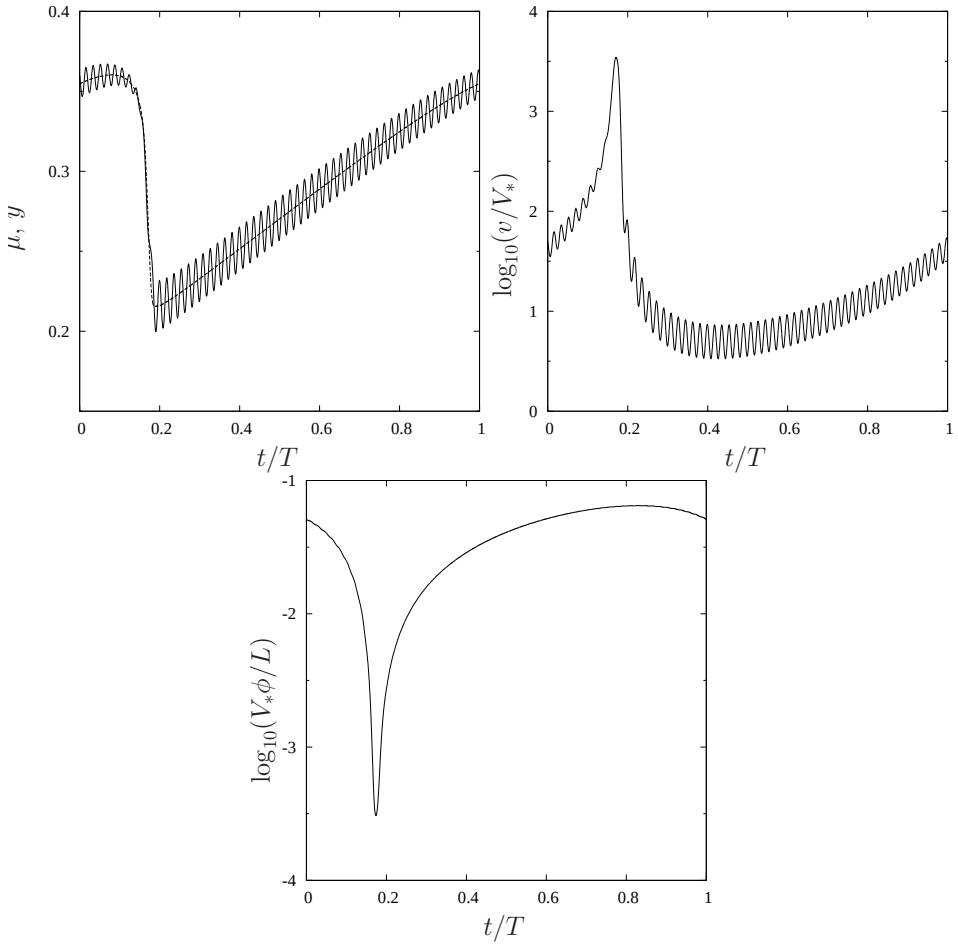

Figure 4: Stable periodic orbit, ODE approximation. The period $T_{\text{ode}} \approx 70.73$. In the upper left figure, the plot that shows the rapid oscillations is that for μ (solid line); the one about which it oscillates is that for y (dashed line). Parameter values: $r = 10^{-2.68} = 0.0021$, $\epsilon = 2.8 \times 10^{-5}$, $V/V_* = 100$.

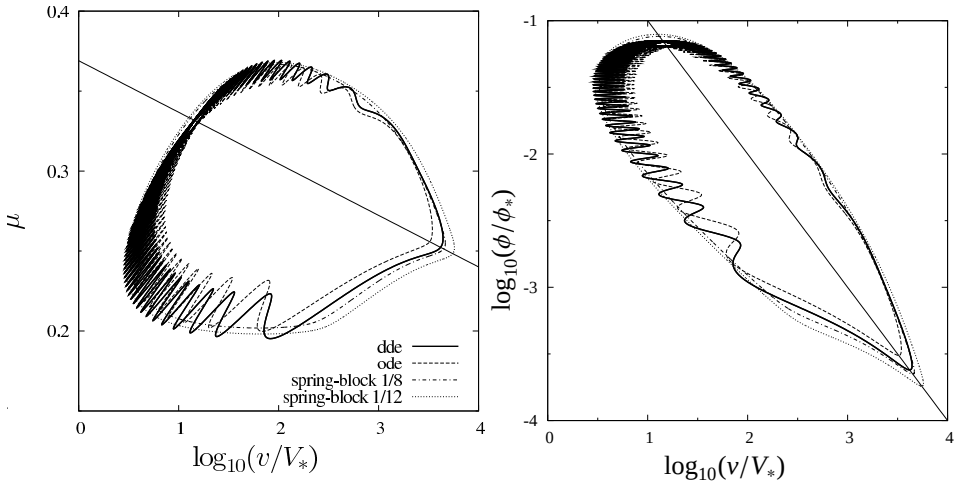

Figure 5: Stable periodic orbit: comparison of results obtained for the exact differential-difference system (31) (solid line) with approximations. Present ODE formulation (17) (dashed line), spring-block system with $M = \rho h/8$ (dash-dotted line), spring-block system with $M = \rho h/12$ (dotted line). Parameter values: $r = 10^{-2.68}$, $\epsilon = 2.8 \times 10^{-5}$, $V/V_* = 100$, $T_{\rm ode} \approx 70.73$, $T_{\rm dde} \approx 73.5$.

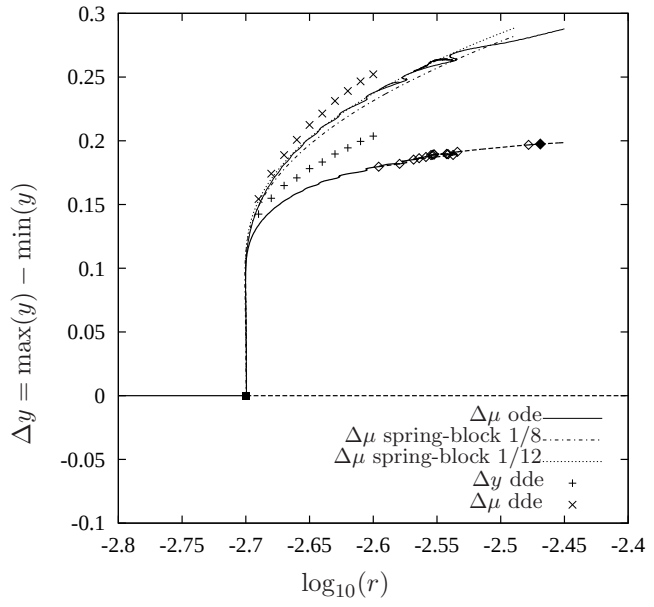

(a)

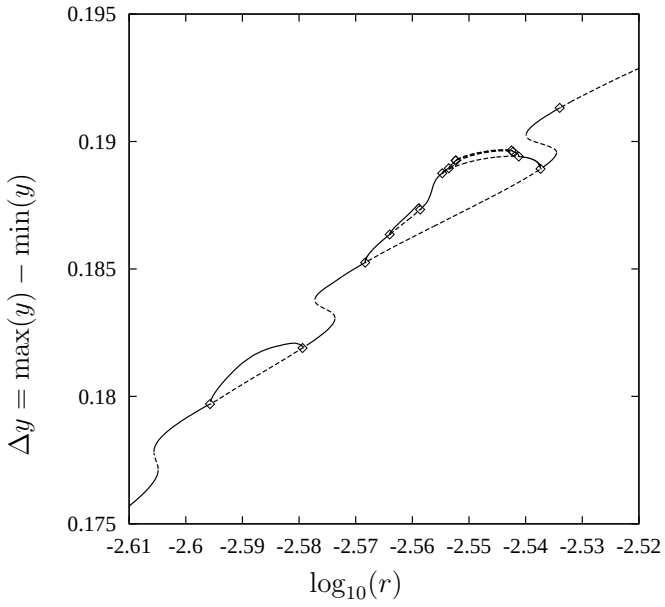

(b)

Figure 6: Bifurcation diagram. The upper figure (a) shows the elastic stress drop amplitude $\Delta y := \max(y) - \min(y)$ for the ODE approximation (thick lines, lower set of curves). The bifurcation points are indicated. Solid square: Hopf bifurcation; open diamonds: period-doubling bifurcation; solid diamond: torus bifurcation of a periodic orbit. For comparison, the upper set of curves (thin lines, see legend) shows estimates of the interfacial stress drop $\Delta\mu$ for the ODE and for the two spring–block systems (for which $\Delta\mu = \Delta y$). Estimates of Δy and $\Delta\mu$ for the DDE are also shown (see legend). The lower figure (b) shows a blow-up of the bifurcation diagram for Δy and represents the amplitude of period-doubled orbits computed with AUTO (solid lines (resp. dashed) correspond to stable (resp. unstable) orbits). Parameter values: $\epsilon = 2.8 \times 10^{-5}$, $V/V_* = 100$.

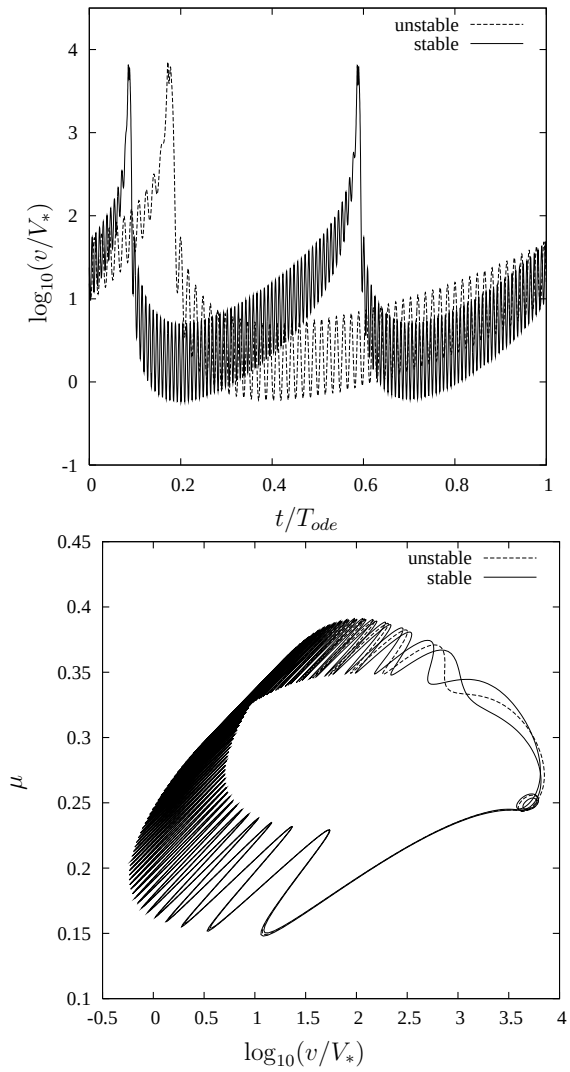

Figure 7: Unstable periodic orbit ($T_{ode} \approx 79.09$) and stable period-doubled orbit ($T_{ode} \approx 158.18$), ODE formulation. Parameter values: $r = 10^{-2.59}$, $\epsilon = 2.8 \times 10^{-5}$, $V/V_* = 100$.

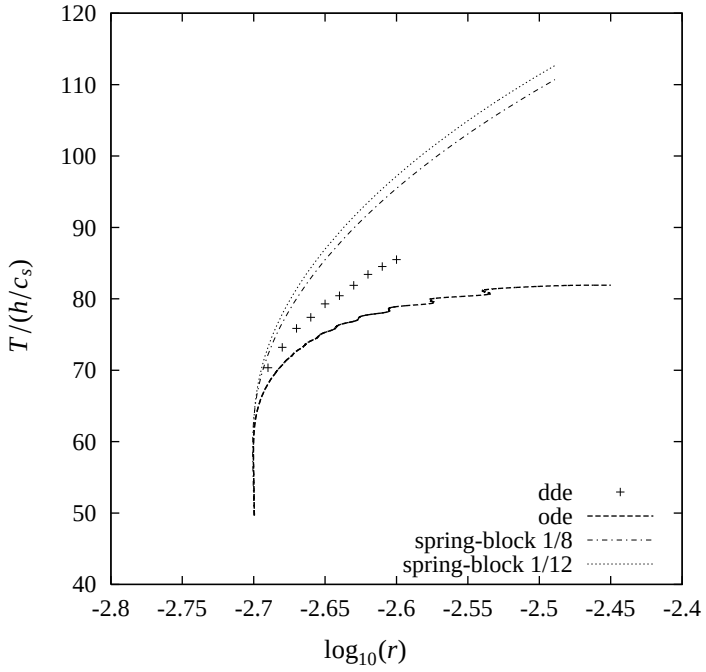

Figure 8: Evolution of the period of the primary periodic orbit for the ODE formulation and the spring–block approximations (see legend). The + symbol represents the estimation of the period for the DDE system computed with RADAR5. Parameter values: $\epsilon = 2.8 \times 10^{-5}$, $V/V_* = 100$.

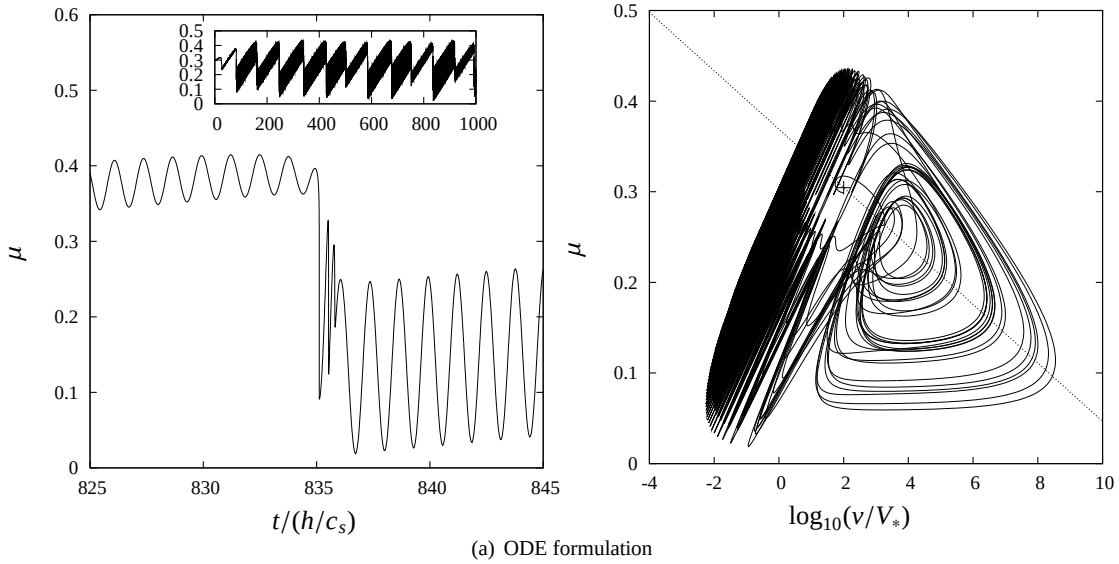

(a) ODE formulation

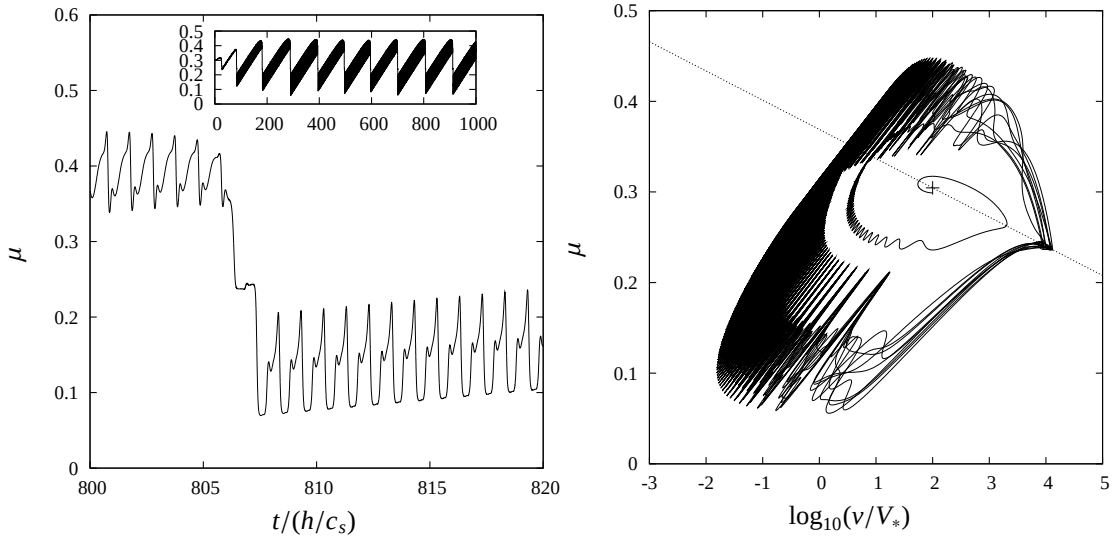

(b) DDE formulation

Figure 9: Comparison of complex dynamics between the ODE and DDE systems from direct numerical time integration. The dotted line and the symbol + correspond to the steady-state line and the location of the friction coefficient value. Parameter values: $r = 10^{-2.3}$, $\epsilon = 2.8 \times 10^{-5}$, $V/V_* = 100$.

List of Tables

Material	a_*	a	b	L [m]	V_* [m/s]	ρ [m kg^{-3}]	G [Pa]	σ [Pa]
paper	0.369	0.0349	0.0489	0.9×10^{-6}	10^{-6}	800	10^{6}	10^{3}
rock	0.6	0.01	0.015	20×10^{-6}	10^{-6}	2500	10^{10}	10^{8}

Table 1: Typical material parameter values used in the Dieterich law (3) (Heslot et al., 1994, Marone, 1998).